

# Simulation of the 6-phase Fractional Pitch Induction Motors to Reduce Harmonic by using the 3-D Finite Element Method

Padej Pao-la-or and Somsak Vacharakup

School of Electrical Engineering, Suranaree University of Technology, Nakhon Ratchasima, Thailand

Email: padej@sut.ac.th, Email: somsak\_v.kup@hotmail.co.th

**Abstract**— This paper presents harmonic reductions of 6-phase induction motors related to increased torque and filtered a sine waveform of magnetic flux density by adjusting coil pitch with the original structure. Full pitch and fractional pitch systems were considered in terms of simulation results and characteristics for optimized applications. There were 2 tools in MATLAB used for these solutions, a 3-D finite element method to do simulations of this system and a Fast Fourier Transform to calculate the harmonic distortion, respectively. The equation used in the simulations is a second order partial differential equation with time-dependent conditions. The results of both full pitch and fractional pitch systems based on steady state and full load of a 6-phase induction motor, 2-pole, 3-HP, squirrel-cage and double-layer motor were obtained. MATLAB was used for 3-D graphics of the simulated 6-phase induction motor.

**Index Terms**—6-phase induction motor, simulation, 3-D finite element method, fractional pitch, harmonic

## I. INTRODUCTION

Over the past 10 years, multi-phase induction motor drives have been developed with more than 3-phases. Three-phase induction motors provide higher torque. A 6-phase power supply can be used for high power drive systems such as ships, airplanes and electric vehicles. Output torque of these multi-phase induction motors is higher than that of 3-phase induction motors. A multi-phase induction motor can be directly used in the form of a 3-phase induction motor, but the performance may not be good if the new stator winding is not designed properly. The important parameters in designing induction motors include torque, output power, vibration, heat generated and harmonic distortion [1-4]. These characteristics depend on the distribution of the magnetic field in the motor [5]. Based on previous research, it was found that 3-phase induction motors can be modified to operate with a 6-phase power supply to act as 6-phase induction motors. Their torque and output power increase can be as much as 1.5-2.0 times, which makes them very attractive since the weight of the motor has not changed. Torque and power can be increased with increasing

numbers of phases, which also lowers the phase current and the electronic switch equipment at a lower current rating. However, the development of a 6-phase induction motors for higher torque applications, leads to higher harmonic distortion. This distortion causes decreased torque and performance [6]. Therefore, the concept of fractional pitch induction motors to reduce harmonic distortion was investigated using Fast Fourier Transforms (FFT) [7-8].

The finite element method is a numerical method commonly used to solve partial differential equations (PDE). It is very widely used in engineering to find solutions of problems concerning electric fields, magnetic fields, heat, and stress distributions, among many others [9-10]. This method will divide regions of the problem into sub-regions composed of nodes and connected by grids. For 3-D problems, the linear tetrahedral element is used to approximate the domain of the problem. Therefore, the current study used a 3-D finite element method (3-D FEM) in the MATLAB environment for simulation to determine the characteristics of this type of induction motor.

## II. THE 6-PHASE INDUCTION MOTOR

Multi-phase induction motor drives can be used directly in the structure of a 3-phase induction motor. Three-phase induction motors, which have two sets of stator windings, are operated as a 6-phase induction motor with a second set of symmetric stator windings. This results in a different phase angle, shifting from the first stator windings by  $60^\circ$  as shown in Fig. 1 [11-12].

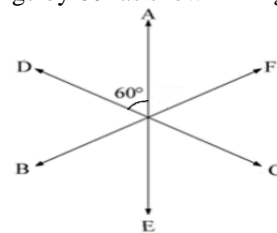


Figure 1. Symmetric type of stator winding

The induction motor structure featuring a 6-phase induction motor, 2-pole, 3-HP, squirrel cages and double-layer motor was used. Details of this motor are given in

Table I. It consists of 36 stator slots with a coil pitch of the stator windings of either full pitch or 16/18 fractional pitch as shown in Figs. 2-3.

TABLE I. PARAMETER OF 6-PHASE INDUCTION MOTOR

Parameter	Value
Output power	3 HP
Voltage	380 V (Star)
Number of poles	2 P
Frequency	50 Hz
Rated speed	2910 rpm
Stator type of winding	Double layer
Stator slot	36
Rotor slot	44
Air gap width	0.4 mm
Number of turns	15 turns

Table I., shows the parameters of a 6-phase induction motor redesigned from the original structure of a 3-phase induction motor, which allowed the voltage and power to remain unchanged. It was found that when applied to a 6-phase system, the poles are less and the speed increases.

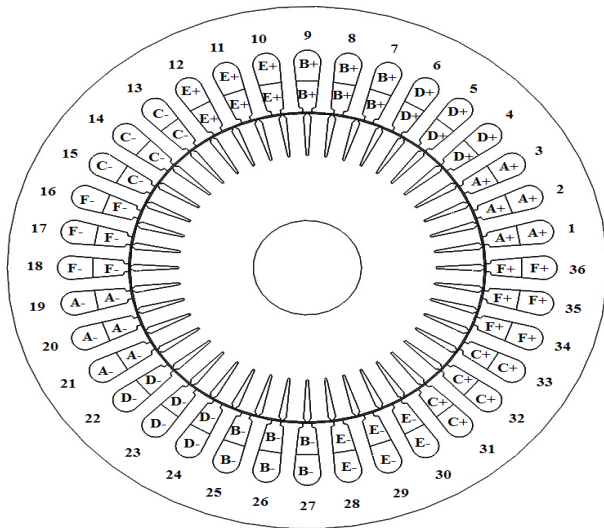


Figure 2. Full pitch stator windings

Fig 2 shows a 6-phase induction motor designed from an original 3-phase structure. The 6-phase concept applied to 3-phase system is divided into 3 steps. In step 1, the 6-phase concept for a 3-phase system can be done by setting the first stator winding position at the number 1 stator slot in the first layer, starting with phases A, D, B, E which are positive poles and phases C, F are negative poles. Then set the phase angle using the symmetry concept with the phase angle of phase D, E, F shifting from phase A, B, C by 60°. Step 2 set the position of the stator windings to the negative pole, starting with

the negative pole phase A with 180° phase angle shift to the positive pole phase A at stator slot number 19 because this motor is a 2-pole system. Then set phases D, E, F with a 60° phase angle increase from phase A, B, C. In the final step, the stator windings will be placed in the second layer by the coil pitch of the stator windings of full pitch. Then set the stator windings to be the same as the first layer, which starts from the negative pole phase A at stator slot number 19 in the second layer.

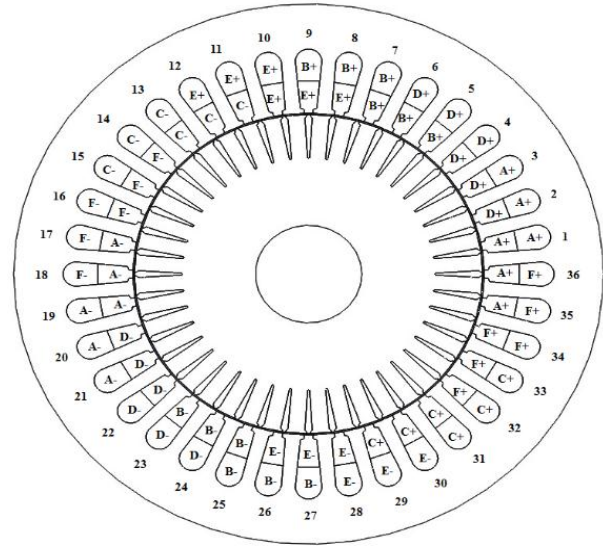


Figure 3. 16/18 Fractional pitch stator windings

Fig 3 shows a 6-phase induction motor designed from an original 3-phase structure of stator windings that is 16/18 fractional pitch. The stator windings will be placed in the second layer by coil pitch of the stator windings at a 16/18 fractional pitch. Then set the stator windings to be the same as the first layer, which starts from the negative pole phase A at stator slot number 17 in the second layer.

### III. MODELING OF MAGNETIC FIELD FOR INDUCTION MOTOR

A magnetic field (**B**) can only be computed by the magnetic vector potential (**A**) represented by (1).

$$\mathbf{B} = \nabla \times \mathbf{A} \tag{1}$$

Mathematical modeling of the magnetic field of the induction motor was done, which induces current in the circuit of the rotor based on the slip (*s*) of the motor. Considering a 3-D motor in an *xyz* plane coordinate, which varies over time and can be calculated using the second order partial differential equation represented by (2).

$$\frac{\partial}{\partial x} \left( \frac{1}{\mu} \frac{\partial A}{\partial x} \right) + \frac{\partial}{\partial y} \left( \frac{1}{\mu} \frac{\partial A}{\partial y} \right) + \frac{\partial}{\partial z} \left( \frac{1}{\mu} \frac{\partial A}{\partial z} \right) - s\sigma \left( \frac{\partial A}{\partial t} \right) + J_0 = 0 \tag{2}$$

$$\text{and } J_0 = \frac{n \cdot I}{a}$$

where  $\mu$  is the magnetic permeability of the magnetic material,  $\sigma$  is the electrical conductivity of the conducting

media in the rotor,  $s$  is the slip of the rotor at a specific operating condition,  $J_0$  is the applied external current density,  $n$  is number of turns,  $I$  is phase of the current and  $a$  is the cross-sectional area of the coil.

Finding the correct solution of the second order partial differential equation shown in (2), is extremely difficult. Therefore, this research used a 3-D finite element method to estimate the solution, which is the most efficient numerical method for solving these types of equations.

#### IV. 3-D FEM FOR INDUCTION MOTOR

##### A. The Element of the System to Study

This research considers a 6-phase induction motor, 2-pole, 3-HP, squirrel cages and double-layer using a finite element method to simulate the distribution of magnetic vector potential and magnetic field. It divides the region of study using linear tetrahedral elements throughout the simulated induction motor in a SolidWorks environment. The dimensions of the induction motor are shown in Fig. 4. A 3-D mesh of the induction motor is shown in Fig. 5. It consists of 42,635 nodes and 220,353 elements.

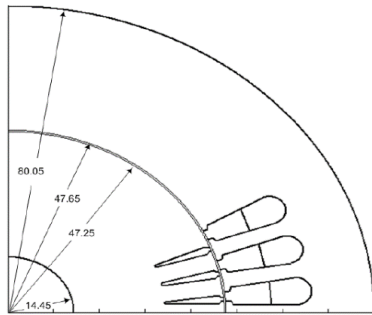


Figure 4. Dimension of induction motor (mm)

Fig. 4 shows a cross section of a 6-phase induction motor showing one quarter of the motor. The figure shows the distance from the center of the stator, rotor, shaft, and air gap between the stator and the rotor. The model of a 6-phase induction motor used in simulation has a double layer stator with 36 slots while the rotor has 44 slots.



Figure 5. The 3-D mesh of induction motor

Fig. 5 A model of a 6-phase induction motor used for simulation with the finite element method. The model

was created in SolidWorks with a tetrahedral mesh. The tetrahedral have nodes in each element and are pyramid shaped.

##### B. The 3-D Finite Element Formulation

The equation of each element uses the Galerkin weighted residual method. In this way, the weighting function is equal to the shape function and the magnetic vector potential at any coordinate can be expressed as (3) [13].

$$A(x, y, z) = A_i N_i + A_j N_j + A_k N_k + A_l N_l \quad (3)$$

In (4)  $N_i$ ,  $i = i, j, k, l$  is the shape function within an element and  $A_i$ ,  $i = i, j, k, l$  is the resulting magnetic vector potential at each node  $i, j, k, l$  of the element.  $V$  is the volume of a linear tetrahedral.

$$N_i = \frac{1}{6V} (a_i + b_i x + c_i y + d_i z) \quad (4)$$

$$V = \frac{1}{6} \begin{vmatrix} 1 & x_i & y_i & z_i \\ 1 & x_j & y_j & z_j \\ 1 & x_k & y_k & z_k \\ 1 & x_l & y_l & z_l \end{vmatrix}$$

And

$$a_i = x_l(y_j z_k - y_k z_j) + x_k(y_l z_j - y_j z_l) + x_j(y_k z_l - y_l z_k)$$

$$a_j = x_l(y_k z_i - y_i z_k) + x_k(y_i z_l - y_l z_i) + x_i(y_l z_k - y_k z_l)$$

$$a_k = x_l(y_i z_j - y_j z_i) + x_j(y_l z_i - y_i z_l) + x_i(y_j z_l - y_l z_j)$$

$$a_l = x_l(y_j z_i - y_i z_j) + x_j(y_i z_k - y_k z_i) + x_i(y_k z_j - y_j z_k)$$

$$b_i = y_l(z_k - z_j) + y_k(z_j - z_l) + y_j(z_l - z_k)$$

$$b_j = y_l(z_i - z_k) + y_i(z_k - z_l) + y_k(z_l - z_i)$$

$$b_k = y_l(z_j - z_i) + y_j(z_i - z_l) + y_i(z_l - z_j)$$

$$b_l = y_k(z_i - z_j) + y_i(z_j - z_k) + y_j(z_k - z_i)$$

$$c_i = x_l(z_j - z_k) + x_j(z_k - z_l) + x_k(z_l - z_j)$$

$$c_j = x_l(z_k - z_i) + x_k(z_i - z_l) + x_i(z_l - z_k)$$

$$c_k = x_l(z_i - z_j) + x_i(z_j - z_l) + x_j(z_l - z_i)$$

$$c_l = x_k(z_j - z_i) + x_j(z_i - z_k) + x_i(z_k - z_j)$$

$$d_i = x_l(y_k - y_j) + x_k(y_j - y_l) + x_j(y_l - y_k)$$

$$d_j = x_l(y_i - y_k) + x_i(y_k - y_l) + x_k(y_l - y_i)$$

$$d_k = x_l(y_j - y_i) + x_j(y_i - y_l) + x_i(y_l - y_j)$$

$$d_l = x_k(y_i - y_j) + x_i(y_j - y_k) + x_j(y_k - y_i)$$

This approach is then applied to the PDE, where the integrations are performed over the element domain ( $\Omega$ ) in (5).

$$\int_{\Omega} N_n \left( \frac{\partial}{\partial x} \left( \frac{1}{\mu} \frac{\partial \mathbf{A}}{\partial x} \right) + \frac{\partial}{\partial y} \left( \frac{1}{\mu} \frac{\partial \mathbf{A}}{\partial y} \right) + \frac{\partial}{\partial z} \left( \frac{1}{\mu} \frac{\partial \mathbf{A}}{\partial z} \right) \right) d\Omega - \int_{\Omega} N_n s \sigma \left( \frac{\partial \mathbf{A}}{\partial t} \right) d\Omega + \int_{\Omega} N_n J_0 d\Omega = 0 \quad (5)$$

Or in compact matrix form

$$[M]_{4 \times 4} \{A\} + [K]_{4 \times 4} \{A\} = \{F\}_{4 \times 1}$$

by

$$[M]_{4 \times 4} = \frac{s\sigma V}{20} \begin{bmatrix} 2 & 1 & 1 & 1 \\ 1 & 2 & 1 & 1 \\ 1 & 1 & 2 & 1 \\ 1 & 1 & 1 & 2 \end{bmatrix}$$

$$[K]_{4 \times 4} = \frac{1}{36\mu V} \begin{bmatrix} b_i b_i + c_i c_i + d_i d_i & b_i b_j + c_i c_j + d_i d_j & & \\ b_j b_i + c_j c_i + d_j d_i & b_j b_j + c_j c_j + d_j d_j & & \\ b_k b_i + c_k c_i + d_k d_i & b_k b_j + c_k c_j + d_k d_j & & \\ b_l b_i + c_l c_i + d_l d_i & b_l b_j + c_l c_j + d_l d_j & & \end{bmatrix}$$

$$\begin{bmatrix} b_k b_k + c_k c_k + d_k d_k & b_l b_l + c_l c_l + d_l d_l \\ b_j b_k + c_j c_k + d_j d_k & b_l b_l + c_l c_l + d_l d_l \\ b_l b_k + c_l c_k + d_l d_k & b_l b_l + c_l c_l + d_l d_l \\ b_l b_k + c_l c_k + d_l d_k & b_l b_l + c_l c_l + d_l d_l \end{bmatrix}$$

$$\{F\}_{4 \times 1} = \frac{J_0 V}{4} \begin{bmatrix} 1 \\ 1 \\ 1 \\ 1 \end{bmatrix}$$

Then, the equations of each of the elements in the region under study are assembled into a system equations. The problem is divided into sub-elements that consist of n nodes. The solution requires the solution of a system of n equations.

The solution to such problems is iterative over a series of short time-steps,  $\Delta t$ , in (6). In this research, the backward difference method was used because this method guarantees convergence even when the results are constantly changing [14].

$$\left( \frac{1}{\Delta t} [M] + [K] \right) \{A\}^{t+\Delta t} = \frac{1}{\Delta t} [M] \{A\}^t + \{F\}^{t+\Delta t} \quad (6)$$

### V. SIMULATION RESULTS AND DISCUSSION

The solution starts from the initial condition of the motor and continues for each rotation of the motor considering the boundary conditions of the problem. This research used an initial condition that the magnetic vector potential (A) at start time is zero. The boundary conditions were applied at the inner surface area of the rotor and the outer surface area of the stator,  $A = 0$ . The conductivity is  $\sigma = 4.90 \times 10^7$  S/m in the rotor bars, and the relative permeability of the stator and rotor cores was  $\mu_r = 5000$ . The free space permeability ( $\mu_0$ ) was  $4\pi \times 10^{-7}$  H/m [15]. In the solution, the motor characteristics consisted of the rotor speed, as shown in Fig. 6. The magnetic vector potential of full pitch and fractional pitch systems during steady state is shown in Figs. 7-12 and magnetic field of full pitch and fractional pitch systems during steady state are shown in Figs. 13-18.

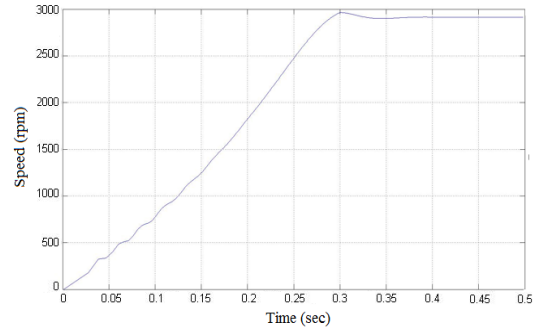


Figure 6. Speed of a 6-phase induction motor

Fig. 6 shows the rotation speed of a 6-phase induction motor from its starting time until reaching steady state. The start time was 0 sec and the motor reached steady state at 0.3 sec as can be seen in the figure. During this time, the speed increased continuously and then the speed was constant.

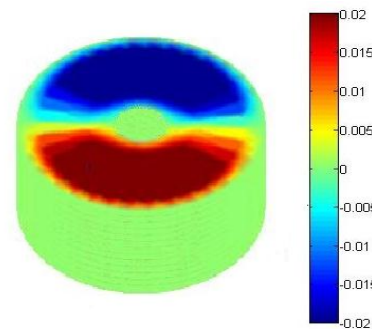


Figure 7. Cross-sectional magnetic vector potential (wb/m) of a full pitch induction motor

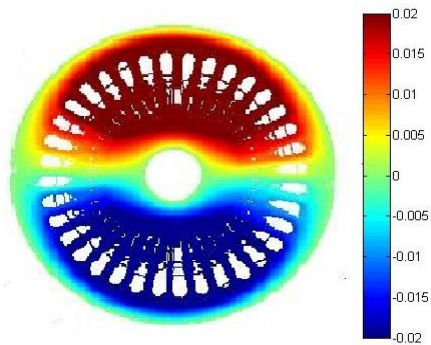


Figure 8. Cross-section of magnetic vector potential (wb/m) at 0° of full pitch of an induction motor

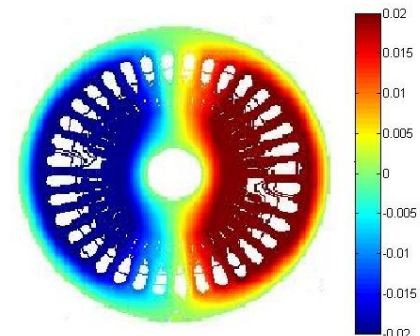


Figure 9. Cross-section of magnetic vector potential (wb/m) at 90° of full pitch in an induction motor

Fig. 7 shows the 3-D model of a 6-phase full pitch induction motor. The vertical axis and graph are fill plotted. In Fig. 8-9 displays the cross-section of a 6-phase induction motor giving the top view with contour plots.

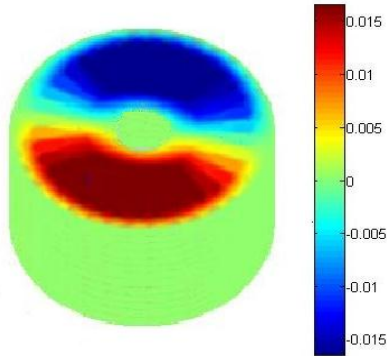


Figure 10. 3-D magnetic vector potential (wb/m) of a fractional pitch induction motor

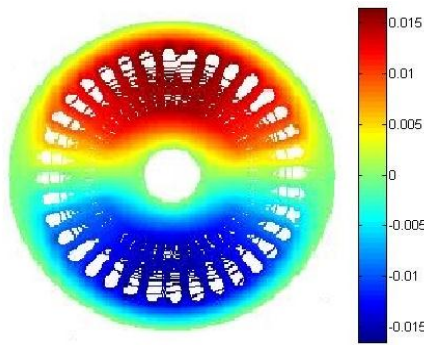


Figure 11. Cross-section of magnetic vector potential (wb/m) at 0° of fractional pitch in an induction motor

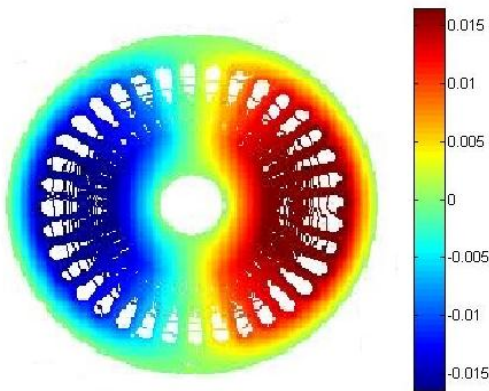


Figure 12. Cross-section of magnetic vector potential (wb/m) at 90° of fractional pitch in an induction motor

Figs. 7-12 show the magnetic vector potential distributed throughout the induction motor for full pitch and fractional pitch systems. The distribution of the magnetic poles shows three ranges. The red range is a positive magnetic vector potential. The blue range is a negative magnetic vector potential and the green range gives positive and negative values that near zero. The

distribution of the colour bars depends on the polarity of the input current in the stator slot. From the distribution of magnetic vector potential, the rotation of each angle of the motor will be slightly different. The full pitch system will have a higher magnetic vector potential than the fractional pitch system at every angle of the motor.

Then the magnetic vector potential is calculated for the magnetic field (1) by considering the motor in 3-D, the  $xyz$  coordinates can be used to calculate the magnetic field along the  $x$ -axis ( $B_x$ ) and the magnetic field along the  $y$ -axis ( $B_y$ ). This is because the current is represented by the  $z$ -axis as is shown in (7) and (8) enabling calculation of the magnetic field [16].

$$B_x = \frac{\partial A_z}{\partial y} = \frac{c_i A_i + c_j A_j + c_k A_k + c_l A_l}{6V} \quad (7)$$

$$B_y = -\frac{\partial A_z}{\partial x} = -\frac{c_i A_i + c_j A_j + c_k A_k + c_l A_l}{6V} \quad (8)$$

$$B = \sqrt{B_x^2 + B_y^2} \quad (9)$$

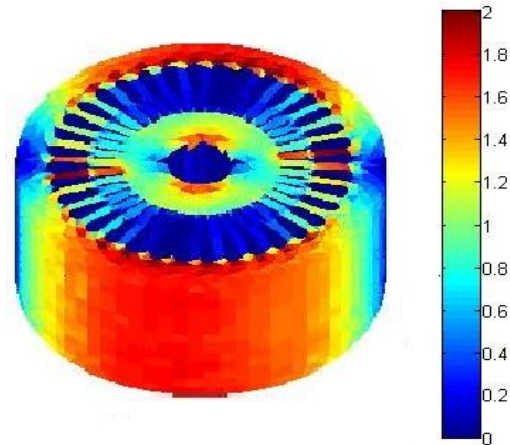


Figure 13. 3-D magnetic field (T) of a full pitch induction motor

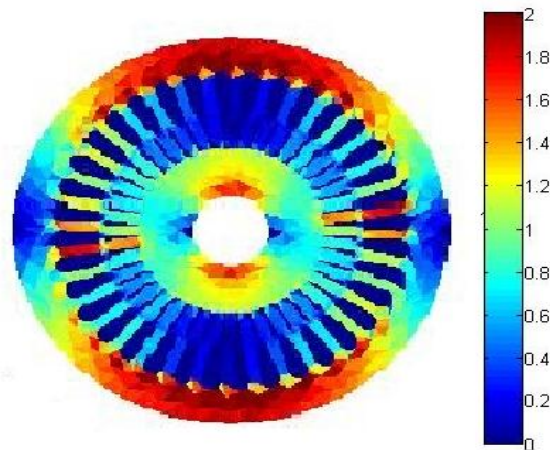


Figure 14. Cross-section of the magnetic field (T) at 0° of a full pitch induction motor

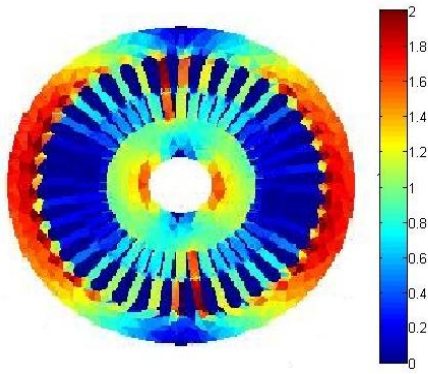


Figure 15. Cross-section of the magnetic field (T) at 90° of a full pitch induction motor

Figs. 13-15 show the 3-D model and cross-section of a 6-phase full pitch induction motor. It shows the vertical axis and top view. The figure was made by fill plotting.

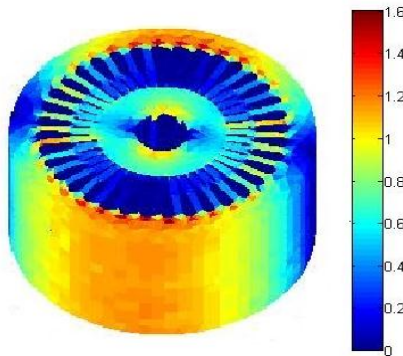


Figure 16. 3-D magnetic field (T) of a fractional pitch induction motor

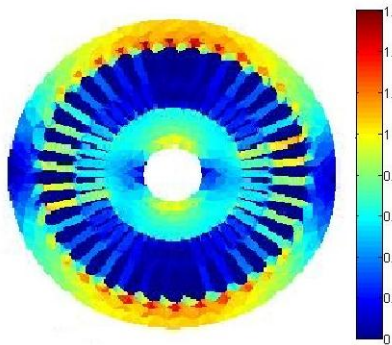


Figure 17. Cross-section of the magnetic field (T) at 0° of a fractional pitch induction motor

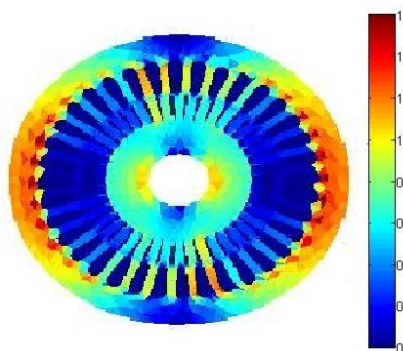


Figure 18. Cross section of the magnetic field (T) at 90° of a fractional pitch induction motor

Figs. 13-18 show the distribution of the magnetic fields. It was found that the distribution of the magnetic field did not occur in the stator slot, but occurred in the iron core. The magnetic vector potential can be seen in Figs. 7-12. The distribution pattern corresponds to the magnetic vector potential. The magnetic field distribution at each angle is slightly different. Based on the simulation, it was found that the magnetic field for the full pitch system was higher than the fractional system. The air gap flux density showed harmonics in the full pitch and fractional pitch systems as is shown in Figs. 19-20.

After calculating the magnetic field in Cartesian coordinates, the coordinate system was converted to cylindrical coordinates. Radial flux density ( $B_r$ ) and tangential flux density ( $B_t$ ) can be expressed as (10)-(11), respectively.

$$B_r = B_x \cos \phi + B_y \sin \phi \quad (10)$$

$$B_t = -B_x \sin \phi + B_y \cos \phi \quad (11)$$

$$B_{ag} = \sqrt{B_r^2 + B_t^2} \quad (12)$$

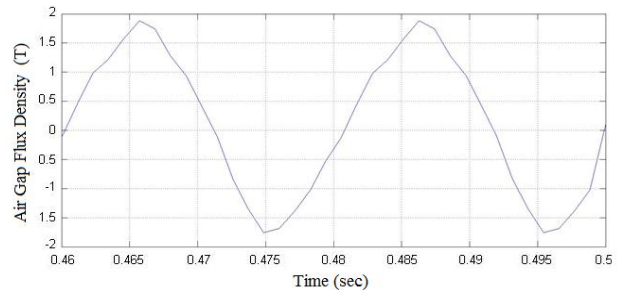


Figure 19. Air gap flux density (T) of a full pitch induction motor

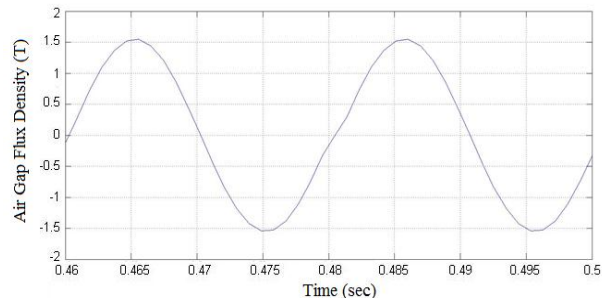


Figure 20. Air gap flux density (T) of a fractional pitch induction motor

Figs. 19-20 show the air gap flux density of a 6-phase induction motor. During steady state, it was found that in the full pitch system, the magnetic flux was higher than the fractional system. Its harmonic distortion was higher as well. It can be observed that the magnetic flux graph does not exhibit a sinusoidal waveform. FFT was applied to the magnetic field data of the induction motor in MATLAB to analyze its harmonic distortion with program. This is shown in Figs. 21-22.

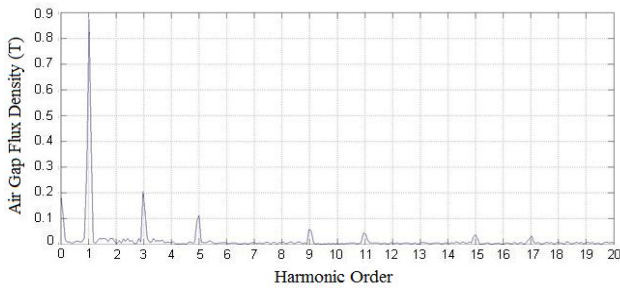


Figure 21. Air gap flux density (T) harmonic distribution of a full pitch induction motor

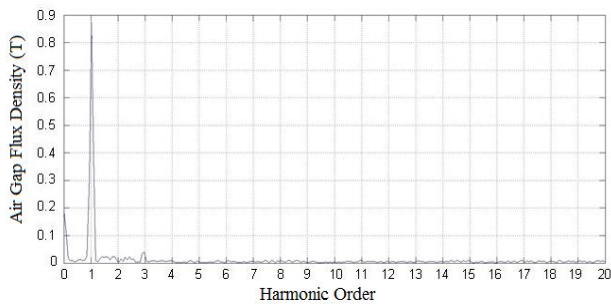


Figure 22. Air gap flux density (T) harmonic distribution of a fractional pitch induction motor

As can be seen from Figs. 21-22 for the full pitch system, harmonic distribution occurred at odd order numbers. In the fractional pitch system, the harmonic distribution decreased. The spectrum of the air gap flux density was calculated to determine %THD. The full pitch system had a THD = 27.35% and the fractional pitch system had THD = 5.42%.

## VI. CONCLUSION

This work studied the characteristics of induction motors, including their magnetic vector potential and magnetic field using a 3-D FEM method and harmonic considerations with a FFT method in MATLAB. A full pitch 6-phase system induction motor was designed to achieve higher magnetic vector potential, magnetic field and harmonic distortion than the fractional pitch system. Therefore, fractional systems will reduce the harmonics. It can be seen that the FEM is a highly accurate method to calculate the characteristics of induction motors and the FFT method can solve the harmonic problem. These are useful designing induction motors for higher efficiency.

## ACKNOWLEDGMENT

This work was supported by School of Electrical Engineering, Institute of Engineering, Suranaree University of Technology.

## REFERENCES

[1] Q. Mingzhong, J. Chao, Z. Yongxin, and L. Geng, "Research on design method and electromagnetic vibration of six-phase fractional-slot concentrated-winding pm motor suitable for ship propulsion," *IEEE Access*, 2017.  
 [2] C. Kim, M. Li, "Torque and ripple analyses of a small BLDC motor for a surgical device," *International Journal of Electrical*

*and Electronic Engineering and Telecommunications (IJEETC)*, vol. 7, no. 1, pp. 16-20, January 2018.  
 [3] S. Shashidhara, P. Raju, "Bearing fault detection of induction motor by ann method," *International Journal of Electrical and Electronic Engineering and Telecommunications (IJEETC)*, vol. 3, no. 1, pp. 34-42, January 2014.  
 [4] A. Uma, "Torque control implementation scheme and back emf ripple reduction using bldc motor," *International Journal of Electrical and Electronic Engineering and Telecommunications (IJEETC)*, vol. 4, pp. 76-84, No. 3, July 2015.  
 [5] T. Dharanirajan, K. Gowri, K. Surya, G. Renukadevil "Open loop response of inverter-fed three-phase induction motor drive," *International Journal of Electrical and Electronic Engineering and Telecommunications (IJEETC)*, vol. 1, no. 1, pp. 148-153, , March 2015.  
 [6] R. Martin, D. Widmer, "Electromagnetic considerations for a six-phase switched reluctance motor driven by a three-phase inverter," *IEEE Transactions on Industry Applications*, vol. 52, no. 5, 2016.  
 [7] H. Shouyi, L. Chuang, Z. Lei, J. Guanming, D. Shangjian, "Mutual coupling and its effect on current and torque of six phases switched reluctance motor," *Eleventh International Conference on Ecological Vehicles and Renewable Energies*, 2016.  
 [8] A. Bao, A. Yong-le, L. Niu, "Study on the air gap flux density of the six-phase induction machine based on trapezoidal phase current waveform with CAD," *International Forum on Information Technology and Applications*, pp. 343-346, 2017.  
 [9] N. Ananthan, N. Vimalraj, G. Kumar, "Design and analysis of brushless dc motor for reduce cogging torque using finite element analysis," *International Journal of Electrical and Electronic Engineering and Telecommunications (IJEETC)*, vol. 1, pp. 35-41, No. 1, March 2015.  
 [10] S. Vacharakup, M. Peerasaksophol, T. Kulworawanichpong, P. Pao-la-or, "Study of natural frequencies and characteristics of piezoelectric transformers by using 3-d finite element method," *Applied Mechanics and Materials*, vols. 110-116, pp. 61-66, 2012.  
 [11] Z. Ping, W. Fan, L. Yu, S. Yi, Y. Bin, "Investigation of a novel 24-slot/14-pole six-phase fault-tolerant modular permanent-magnet in-wheel motor for electric vehicles," *Energies*, 2013.  
 [12] L. Chih, H. Chang, "Multiobjective optimization design for a six-phase copper rotor induction motor mounted with a scroll compressor," *IEEE Transactions on Magnetics*, vol. 52, no. 7, 2016.  
 [13] W. Lewis, P. Nithiarasu, N. Seetharamu, "Fundamentals of the Finite Element Method for Heat and Fluid Flow," John Wiley & Sons, USA, 2004.  
 [14] A. Jabbar, N. Phyu, J. Liu, C. Bi, "Modeling and numerical simulation of brushless permanent-magnet dc motor in dynamic condition by time-stepping technique," *IEEE Transaction on Industrial Application*, vol. 40, No. 3, pp. 763-769, 2004.  
 [15] A. Bunmat, P. Pao-la-or, "Analysis of magnetic field effects operators working a power transmission line using 3-d finite element method," *The 18th International Conference on Electrical Machines and Systems (ICEMS 2015)*, Pattaya, Thailand, pp. 1187-1191, October 2015.  
 [16] P. Pao-la-or, A. Isaramongkolrak, T. Kulworawanichpong, "Finite Element Analysis of Magnetic Field Distribution for 500-kV Power Transmission Systems," *Engineering Letters*, vol. 18, no. 1, pp. 1-9, 2010.



**Padej Pao-la-or** is an associate professor of the School of Electrical Engineering, Institute of Engineering, Suranaree University of Technology, Nakhon Ratchasima, THAILAND. He received B. Eng. (1998), M. Eng. (2002) and D. Eng. (2006) in Electrical Engineering from Suranaree University of Technology, Thailand. His fields of research interest include a broad range of power systems, finite element analysis, optimization and artificial intelligence, electromagnetic field, electrical machinery and energy conversion. He has joined the school since December 2005 and is currently a member in Power System Research, Suranaree University of Technology.



**Somsak Vacharakup** is a student of the School of Electrical Engineering, Institute of Engineering, Suranaree University of Technology, Nakhon Ratchasima, THAILAND. He received B. Eng. (2008), M. Eng. (2011) in Electrical Engineering from Suranaree University of Technology, Thailand. His fields of research interest include a broad range of finite element method, electromagnetic field, electrical machinery and energy conversion.